

SMARTY: The mileS Moderate resolution neAr-infRared sTellar librarY

Michele Bertoldo-Coêlho^{1*}, Rogério Riffel^{1,2}, Marina Trevisan¹, Natacha Zanon Dametto^{1,2}, Luis Dahmer-Hahn⁴, Paula Coelho⁵, Lucimara Martins⁶, Daniel Ruschel-Dutra⁷, Alexandre Vazdekis^{2,3}, Alberto Rodríguez-Ardila^{8,9}, Ana L. Chies-Santos¹, Rogemar A. Riffel¹⁰, Francesco La Barbera¹¹, Ignacio Martín Navarro^{2,3}, Jesus Falcon Barroso^{2,3}, Tatiana Moura⁵

¹Departamento de Astronomia, Instituto de Física, Universidade Federal do Rio Grande do Sul, Av. Bento Gonçalves 9500, 91501-970 Porto Alegre, RS, Brazil

²Instituto de Astrofísica de Canarias, E-38205 La Laguna, Tenerife, Spain

³Universidad de La Laguna, Dpto. Astrofísica, E-38206 La Laguna, Tenerife, Spain

⁴Shanghai Astronomical Observatory, Chinese Academy of Sciences, 80 Nandan Road, Shanghai 200030, China

⁵Universidade de São Paulo, Instituto de Astronomia, Geofísica e Ciências Atmosféricas, Rua do Matão 1226, 05508-090, São Paulo, Brazil

⁶NAT – Universidade Cidade de São Paulo/Universidade Cruzeiro do Sul, Rua Galvão Bueno 868, São Paulo-SP, 01506-000, Brazil

⁷Departamento de Física, Universidade Federal de Santa Catarina, P.O. Box 476, 88040-900, Florianópolis, SC, Brazil

⁸Laboratório Nacional de Astrofísica, Rua dos Estados Unidos, 154, 37504-364 Itajubá, MG, Brazil

⁹Instituto Nacional de Pesquisas Espaciais, Av. dos Astronautas, 1758 - Jardim da Granja São José dos Campos/SP - 12227-010, Brazil

¹⁰Departamento de Física, Centro de Ciências Naturais e Exatas, Universidade Federal de Santa Maria, 97105-900, Santa Maria, RS, Brazil

¹¹INAF - Osservatorio Astronomico di Capodimonte, sal. Moiariello 16, Napoli, 80131, Italy

arXiv:2404.14530v1 [astro-ph.GA] 22 Apr 2024

ABSTRACT

Most of the observed galaxies cannot be resolved into individual stars and are studied through their integrated spectrum using simple stellar populations (SSPs) models, with stellar libraries being a key ingredient in building them. Spectroscopic observations are increasingly being directed towards the near-infrared (NIR), where much is yet to be explored. SSPs in the NIR are still limited, and there are inconsistencies between different sets of models. One of the ways to minimize this problem is to have reliable NIR stellar libraries. The main goal of this work is to present SMARTY (mileS Moderate resolution neAr-infRared sTellar librarY) a $\sim 0.9 - 2.4 \mu\text{m}$ stellar spectral library composed of 31 stars observed with the Gemini Near-IR Spectrograph (GNIRS) at the 8.1 m Gemini North telescope and make it available to the community. The stars were chosen from the MILES library, for which the atmospheric parameters are reliable (and well tested), to populate different regions of the Hertzsprung–Russell (HR) diagram. Furthermore, five of these stars have NIR spectra available that we use to assess the quality of SMARTY. The remaining 26 stars are presented for the first time in the NIR. We compared the observed SMARTY spectra with synthetic and interpolated spectra, finding a mean difference of $\sim 20\%$ in the equivalent widths and $\sim 1\%$ in the overall continuum shape in both sets of comparisons. We computed the spectrophotometric broadband magnitudes and colours and compared them with the 2MASS ones, resulting in mean differences up to 0.07 and 0.10 mag in magnitudes and colours, respectively. In general, a small difference was noted between the SMARTY spectra corrected using the continuum from the interpolated and the theoretical stars.

Key words: stars: general – galaxies: stellar content – catalogs – techniques: spectroscopic

1 INTRODUCTION

Galaxies in the local universe are the final product of a very long process, which depends on a combination of internal (e.g. star formation, stellar and chemical evolution) and external processes (e.g. environment). They display a wide range of properties, such as luminosities, stellar masses, gas, and dust content (e.g. Conselice 2014; Sánchez et al. 2018; Sánchez 2020; Sánchez et al. 2021; Riffel et al. 2021, 2022, 2023). The determination of many of these properties relies on the correct characterisation of their stellar content, which, in turn, depends on reliable stellar population models. One of the most common ways of modelling integrated stellar populations is through

spectral fitting, which can, for example, combine simple stellar populations (SSPs) in different proportions to build the composite stellar population that best describes the observed galaxy (Tinsley 1968; Fernandes et al. 2005; Walcher et al. 2011; Conroy 2013; Gomes & Papaderos 2017; Cappellari 2023). Thus, the SSPs are the most important ingredient in this type of characterisation.

To build up reliable SSP models, one needs several ingredients. Stellar libraries are one of the most fundamental ones (e.g. Worthey et al. 1992; McWilliam 1997; Sánchez-Blázquez et al. 2006; Gustafsson et al. 2008; Husser, T.-O. et al. 2013; Coelho 2014; Chen et al. 2014; Villaume et al. 2017; Knowles et al. 2021, and references therein), and can be either theoretical or empirical. Empirical libraries depend on existing observed stellar spectra, for which high signal-to-noise data can be obtained only for nearby stars. Thus, em-

* E-mail: michele.bertoldo@ufrgs.br

pirical libraries are restricted to nearby and bright objects, leading to libraries biased to metallicity and abundance ratios of stars in the solar neighbourhood. Besides, these libraries have limited coverage of atmospheric parameters and spectral resolution. Theoretical libraries, on the other hand, can encompass a wide range of parameters, including the possibility of high-resolution spectra. However, these libraries depend on our knowledge of the physics of stellar atmospheres and data of atomic and molecular opacities. Thus, both are important since they complement each other, not only in their use but in their assembly. For instance, theoretical libraries are tested and calibrated using empirical libraries (Coelho 2009; Arentsen et al. 2019; Coelho et al. 2020; Lançon et al. 2021) while empirical libraries rely on theoretical libraries for estimating the atmospheric parameters of stars. Both types of libraries have been intensely evolving in the last years and, at least in the optical, can confidently be used to reproduce the integrated spectra of stellar systems (Martins et al. 2019; see also Moura et al. 2019; Rennó et al. 2020).

Ideally, for a given set of atmospheric parameters, theoretical and empirical spectra should be equivalent; however, a complete understanding of stellar physics (as well as atmospheric, atomic, and molecular parameters) and greater observational power would be necessary for this scenario to be achieved. A way to overcome this is to use combined empirical and theoretical stellar libraries. For instance, Westera et al. (2002) used empirical data to correct the spectral energy distributions of the Basel Stellar Library (BaSeL). Coelho (2014) used observed stellar spectra to test her theoretical stellar library. Empirical and theoretical stellar libraries can also be used to build semi-empirical stellar population synthesis models in methods called differential stellar population (Walcher et al. 2009) and flexible SPS (FSPS, Conroy et al. 2009), as well as in abundance ratio variations (e.g. Knowles et al. 2021, 2023).

Studies of the stellar content of galaxies using the near-infrared (NIR) bands can date back to the 80's (Rieke et al. 1980). However, they are becoming more popular over the last years (e.g. Origlia et al. 1997; Maraston 2005; Riffel et al. 2006, 2007; Silva et al. 2008; Riffel et al. 2008, 2009, 2011a,b; Maraston & Strömbäck 2011; Kotilainen et al. 2012; Vazdekis et al. 2012; Zibetti et al. 2013; Martins et al. 2013a,b; Dametto et al. 2014; Riffel et al. 2015; Vazdekis et al. 2016; Röck et al. 2016, 2017; Dahmer-Hahn et al. 2018; Dahmer-Hahn et al. 2019; Riffel et al. 2019; Eftekhari et al. 2021, 2022; Riffel et al. 2022; Gasparri et al. 2021, 2024) mostly because the detectors have improved in this spectral region and telluric corrections became more efficient (e.g. Smette et al. 2015).

Additionally, understanding the stellar populations using the NIR spectral region is now of utmost importance since the JWST is producing amazing data in this spectral region (e.g. Luhman et al. 2024; Marino et al. 2024; Boyett et al. 2024). This spectral region is interesting since it is less affected by dust extinction than the optical, allowing the study of the light content inside optically obscured regions (e.g. Riffel et al. 2006, 2015; Riffel et al. 2019, and references therein). Besides that, models have predicted that cold evolved stars dominate the NIR emission in galaxies. In particular, the thermally pulsing asymptotic giant branch (TP-AGB), phase of cold, intermediate-mass giants stars of difficult modelling, is believed to contribute up to 80% in K band luminosity for intermediate-age populations (0.2 – 2 Gyr) (Maraston et al. 2006; Salaris et al. 2014), but with a limited impact on the spectral features (Riffel et al. 2015; Röck et al. 2017; Eftekhari et al. 2021, 2022). See, for example, Vero et al. (2022b) for a discussion on the effect of these stars in the building of SSP models.

The path towards developing robust SSP models involves comparing empirical and synthetic stellar spectral libraries across the

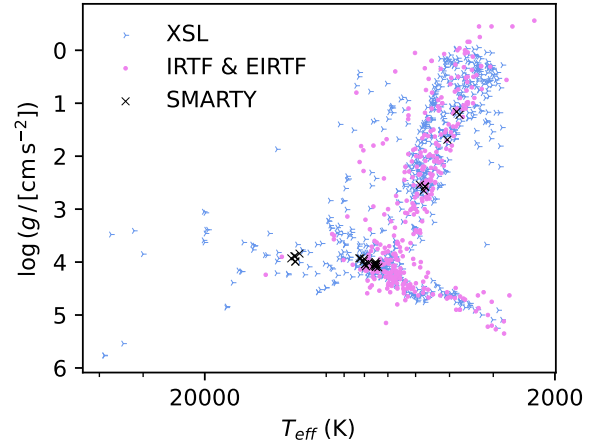


Figure 1. Parameter coverage of existing empirical NIR stellar libraries in the $\log g$ vs. T_{eff} plane. The blue markers and the violet dots are the stars from XSL (683 stars with $R \sim 10\,000$; Chen et al. 2014; Gonneau et al. 2020; Vero et al. 2022a) and IRTF+EIRTF (210+287 stars with $R \sim 2\,000$; Cushing et al. 2005; Rayner et al. 2009; Villaume et al. 2017), respectively. The stars presented in this work are indicated by the black crosses (31 stars with $R \sim 1\,300$).

wavelength ranges of photospheric emission. For instance, the theory of stellar physics enters all SSP models, even when this is only implicit in the association of fundamental stellar parameters with empirical spectral library stars (Lançon et al. 2021). To shed some light on our understanding of the stellar populations in the NIR spectral regions, two aspects are thus fundamental: *i*) expand the existing stellar libraries on the NIR since they do not completely populate the HR diagram (e.g. Cushing et al. 2005; Rayner et al. 2009; Meneses-Goytia et al. 2015; Röck et al. 2016; Villaume et al. 2017; Lançon et al. 2021) and *ii*) to fine-tune the NIR theoretical libraries, comparing them with the empirical stellar libraries (e.g. Coelho 2014).

Aimed at helping to overcome these problems, here we present a new set of NIR stellar spectra of a sub-sample of MILES stars (Sánchez-Blázquez et al. 2006; Falcón-Barroso et al. 2011), whose atmospheric parameters have been previously determined (Cenarro et al. 2007; García Pérez et al. 2021). For this purpose, we selected a sub-sample of stars from the MILES stellar library, which have been used to test theoretical stellar spectra in the optical region by Coelho (2014, see § 2 for more details). For the selected MILES stars, we obtained the NIR data using the Gemini Near-IR Spectrograph (GNIRS) on the Gemini North telescope, from ~ 0.9 to ~ 2.4 μm at a moderate spectral resolution ($R \sim 1\,300$).

This paper is organised as follows: in Sect. 2, we describe the sample selection, our Gemini observations and data reduction. In Sect. 3, we describe the processes applied to calibrate the flux in order to fine-tune the spectra quality. Finally, our last remarks are given in Sect. 4.

2 DATA

2.1 Sample Selection

Our sample selection was based on a systematic comparison between the MILES optical observations and a grid of synthetic spectra available in Coelho (2014). This author grouped the MILES stars in bins of T_{eff} and $\log g$ with widths given by the uncertainties in these

parameters. Our intention was to have from 6 to 8 stars for each $\log g$ and [Fe/H] with effective temperature varying around 100 K to help correct absorption lines of synthetic spectra. However, due to limitations of observing time, we were able to observe only a sub-sample of these stars. We selected the stars giving priority to hotter stars, which are lacking in the IRTF (Infrared Telescope Facility Spectral Library; contains 210 stars within 0.8 – 5.4 μm with medium-resolution $R \sim 2000$ observed with the cross-dispersed spectrograph SpeX from the NASA Infrared Telescope Facility on Mauna Kea, Hawaii; Cushing et al. 2005; Rayner et al. 2009) and EIRTF libraries (Extended IRTF Spectral Library; contains 287 stars observed with the SpeX within 0.7 – 2.5 μm with $R \sim 2000$; Vilamaire et al. 2017), and also to have a diverse distribution on the HR diagram.

The final sample comprises 31 stars listed in Tab. 1. The sample is well distributed in the atmospheric parameter space (see Fig. 1) and with data available in the optical. Of this sample, 5 stars are common with other NIR libraries (IRTF, EIRTF, and XSL, the X-shooter Spectral Library; contains 683 stars within 0.35 – 2.48 μm with moderate-to-high resolution $R \sim 10000$ observed with the X-shooter three-arm spectrograph of the Very Large Telescope on Cerro Paranal, Chile; Chen et al. 2014; Gonneau et al. 2020; Vero et al. 2022a) to be used as a control sample, and 26 are observed for the first time in the NIR. The spectra in the optical region (3 525–7 500 Å) are available in the MILES library (Sánchez-Blázquez et al. 2006; Falcón-Barroso et al. 2011) with a resolution of 2.5 Å (in FWHM), while the NIR spectral range was observed with GNIRS at $R \sim 1300$. A comprehensive description of the observation process and data reduction is provided in § 2.2.

2.2 Observations and data reduction

The NIR spectra were obtained using the cross-dispersed (XD) mode of GNIRS on the 8.1 m Gemini North telescope in Mauna Kea, Hawaii. With the “long blue” camera with the LXD prism, 10 l/mm grating and 0.10” wide slit, this mode gives simultaneous spectral coverage from ~ 0.83 – 2.5 μm at $R \sim 1300$ with a pixel scale of 0.05”/pix. To remove the sky emission, the targets have been observed in the ABBA-type pattern, with the source always on the slit. One telluric star per object was observed (either before or after the observations) to remove the telluric bands that plague the NIR spectral range. Individual and total exposure times varied depending on the object’s brightness and the likely observing conditions (see below) and are given in Tab. 2.

The slit was orientated close to the mean parallactic angle during the observations of both the science target and standard star. This procedure was adopted to minimise the effects of differential atmospheric refraction, which can be important over this wide wavelength range, especially at low elevations.

The data were acquired in queue mode between 2016 and 2017. Observations were taken from standard queue programs (GN-2016B-Q-76, GN-2017A-Q-66 – PI: R. Riffel).

Data reduction was carried out by a slightly modified version of XDGNIRS (Mason et al. 2015) pipeline, V1.9, which is available at <https://xdgnirs.readthedocs.io/en/latest/>. Standard CCD procedures, such as bias subtraction, flat-fielding, and wavelength calibration, were followed and implemented via customary IRAF (Tody 1986) tasks. Uncertainties were estimated from electron counts due to the science targets and atmospheric emission, as well as characteristic read noise and dark current values of the detector.

The two most critical aspects of the data reduction were removing

Table 1. Stellar atmospheric parameters and other information for the SMARTY stars.

Star	T_{eff} K	$\log g$ $\log [\text{cm s}^{-2}]$	[Fe/H]	E(B – V)	Spec. Type
(1)	(2)	(3)	(4)	(5)	(6)
HD 015798	6527	4.07	-0.12	0.000	F5V
HD 026322	7008	3.94	0.13	0.003	F2IV-V
HD 027295 ^a	11034	3.99	-0.11	0.000	B9IV
HD 029375	7240	3.93	0.13	0.053	F0V
HD 071030	6541	4.03	-0.15	0.000	F6V
HD 078234	6976	4.04	-0.06	0.014	F2V
HD 087822 ^b	6573	4.06	0.10	0.018	F4V
HD 113022	6491	4.09	0.11	0.000	F6Vs
HD 114642	6491	4.04	-0.04	0.000	F6V
HD 121299	4695	2.58	0.10	0.019	K2III
HD 137391 ^c	7186	3.93	0.10	0.004	F0V
HD 142908	7038	3.98	-0.02	0.004	F0IV
HD 143807	10727	3.84	-0.01	0.024	A0p...
HD 145976 ^c	6927	4.08	-0.02	0.018	F3V
HD 149121	11099	3.89	0.03	0.007	B9.5III
HD 155078	6508	4.00	0.03	0.032	F5IV
HD 157856	6523	4.04	-0.07	0.000	F3V
HD 166285	6389	4.10	-0.06	0.000	F5V
HD 169027	11030	3.89	-0.08	0.031	A0
HD 172103	6815	4.01	0.03	0.086	F1IV-V
HD 173524	11323	3.93	0.10	0.015	B9.5p...
HD 173667	6458	4.04	0.01	0.000	F6V
HD 194943	6971	4.04	-0.01	0.006	F3V
HD 205512 ^c	4703	2.57	0.03	0.000	K1III
HD 206826	6490	4.09	-0.11	0.000	F6V
HD 207130	4741	2.65	0.08	0.010	K0III
HD 209459	11015	3.99	-0.07	0.052	B9.5V
NGC 7789 415	3815	1.16	0.01	0.269	GB
NGC 7789 501	4057	1.69	0.01	0.269	GB
NGC 7789 637	4857	2.54	0.01	0.269	-
NGC 7789 971	3746	1.22	0.01	0.269	GB

Table Notes: (1) star identification; (2) effective temperature; (3) superficial gravity; (4) metallicity; (5) extinction parameter and (6) spectral type. (2)–(4) were obtained from Prugniel et al. (2011); Sharma et al. (2016) and (5)–(6), from Sánchez-Blázquez et al. (2006). The superscript letter after the control star name identifies the library in which it is also present: ^a in XSL; ^b in IRTF; and ^c in EIRTF.

telluric features and matching the sensitivity function between different orders. Regarding the former, the reference spectrum of telluric standards was first treated with an algorithm to remove hydrogen lines from the star’s atmosphere based on a direct comparison with a high-resolution and high signal-to-noise spectrum of Vega. As for the latter, scale factors for small multiplicative corrections between the sensitivity functions of different diffraction orders were estimated by minimising the quadratic difference between overlapping regions of the spectrum. The same telluric standard star was used for flux calibration.

3 DATA QUALITY

Many of the SMARTY observations at Gemini were carried out under poor weather conditions (see Tab. 2). Despite that, we achieved a good telluric correction, but we needed to apply an independent flux calibration to our data in order to correct the ‘steps’ in the continuum. These irregularities likely stem from challenges to match the sensitivity function of different orders. The independent flux calibration was performed according to the following procedures. First, we normalised the SMARTY spectra, leading to a spectrum of pure absorption features, F_{norm} . We then multiplied the normalised spectra by the continuum flux, F_C , from a reference spectra, using:

(i) **common stars:** Five SMARTY stars have NIR spectra available from other empirical libraries, namely: HD 027295 ($T_{\text{eff}} = 11\,034$ K; in XSL), HD 087822 ($T_{\text{eff}} = 6\,573$ K; in IRTF), HD 137391,

Table 2. Observation log for the SMARTY stars.

Star	RA °	DEC °	Airmass	ExpTime s	Observations #	ImQuality %-ile	Cloud Cover %-ile	Background %-ile	Water Vapour %-ile
(1)	(2)	(3)	(4)	(5)	(6)	(7)	(8)	(9)	(10)
HD 015798	38.0218	-15.24467	1.228	1.2	8	70	50	Any	80
HD 026322	62.7078	26.48095	1.073	2.7	12	70	70	20	80
HD 027295	64.8587	21.14231	1.293	5.5	12	20	70	Any	Any
HD 029375	69.5393	16.03329	1.019	4.0	12	70	50	20	20
HD 071030	126.4578	17.04627	1.143	4.3	12	70	70	Any	Any
HD 078234	137.0173	32.54040	1.125	5.7	12	70	70	Any	20
HD 087822	152.0662	31.60405	1.582	4.7	8	70	50	50	50
HD 113022	195.1613	18.37301	1.168	7.0	12	70	50	50	80
HD 114642	198.0148	-16.19860	1.242	2.5	12	70	70	Any	80
HD 121299	208.6756	-1.50312	1.321	1.1	12	70	50	Any	50
HD 137391	231.1226	37.37716	1.074	1.5	12	70	50	50	Any
HD 142908	238.9483	37.94696	1.159	3.5	12	70	50	20	Unknown
HD 143807	240.3607	29.85106	1.187	5.5	12	70	50	80	80
HD 145976	243.1895	26.67058	1.144	6.0	12	70	50	80	80
HD 149121	248.1487	5.52122	1.033	8.5	8	70	70	Any	80
HD 155078	257.4498	-10.52330	1.321	3.7	12	70	50	Any	80
HD 157856	261.4911	-1.65178	1.108	8.5	12	70	70	20	Any
HD 166285	272.4751	3.11983	2.228	3.0	8	20	70	Any	Any
HD 169027	274.2447	68.74146	1.686	19.0	12	20	70	50	Any
HD 172103	279.5792	-1.11299	1.944	7.0	12	70	50	Any	Any
HD 173524	280.6581	55.53946	1.732	3.7	12	20	50	Any	Any
HD 173667	281.4155	20.54631	1.842	1.0	8	70	50	Any	Any
HD 194943	307.2151	-17.81369	1.570	1.2	12	20	70	Any	Any
HD 205512	323.6940	38.53406	1.177	0.8	8	70	70	80	Any
HD 206826	326.0358	28.74261	1.162	1.0	12	20	70	80	Any
HD 207130	325.7668	72.32009	1.685	1.0	4	70	70	80	80
HD 209459	330.8293	11.38655	1.133	7.5	12	70	70	80	Any
NGC 7789 415	359.2636	56.76609	1.530	13.5	12	70	70	Any	50
NGC 7789 501	359.2964	56.74142	1.404	45.0	12	70	70	Any	20
NGC 7789 637	359.3435	56.69611	1.253	120.0	4	70	50	Any	50
NGC 7789 971	359.4649	56.64907	1.402	15.0	12	70	70	Any	50

Table Notes: (1) star identification; (2) right ascension in degrees; (3) declination in degrees; (4) relative air mass; (5) exposure time (6) number of exposures (7) image quality in percentile; (8) cloud cover in percentile; (9) background in percentile when the information is provided; (10) water vapour in percentile when the information is provided.

HD 145976 and HD 205512 ($T_{\text{eff}} = 7\,186, 6\,927$ and $4\,703$ K, respectively; in EIRTF). The shape of the continuum of these stars has been used as a reference to fine-tune the flux calibration of the SMARTY counterpart. Note that these stars have a good T_{eff} coverage.

(ii) **interpolated stars:** For all SMARTY stars, we have done the independent flux calibration using the e-MILES interpolator (see Vazdekis et al. 2003, 2016, for more details) to interpolate among 180 IRTF plus 200 EIRTF stellar spectra to compute a spectrum which best matches the SMARTY stars stellar parameters adopting a local interpolation scheme¹. Therefore, as IRTF+EIRTF do not have a significant number of stars hotter than $\sim 7\,000$ K, the interpolated corrected flux is not recommended for stars above this temperature since the box can be bigger than typical uncertainties in the determination of the parameters.

(iii) **synthetic stars:** Following Coelho et al. (2020), we computed synthetic spectra for the 31 SMARTY stars using as input the values computed by Prugniel et al. (2011) and Sharma et al. (2016) for effective temperature and surface gravity, and approximated values of metallicity ($[\text{Fe}/\text{H}] = -0.1, 0.0$ or 0.2). The continuum of these stars has been used as a reference for the independent flux calibration.

¹ The interpolator selects stars whose parameters are within a box around the requested parametric point ($T_{\text{eff}}, \log g, [\text{Fe}/\text{H}]$), which is divided into eight boxes. If no stars are found in any of these boxes, it can be expanded up to a limit. Thus, the larger the density of stars around the point, the smaller the box is.

It is worth noting that the spectra of colder ($T_{\text{eff}} < 6\,000$ K) are not well predicted by the models².

To fit the continuum, we smoothed the spectra using LOESS³, discarding the low flux values (i.e., the absorption features) from the spectra in each iteration by adopting different values for the lower and upper σ -clipping factors. This process was repeated until only the data points of the continuum were left to be fitted. To properly fit the continuum of different spectral regions, the fit was done independently within wavelength ranges, as illustrated in Fig. 2. The whole procedure was performed interactively by visually inspecting the fits and changing the fitting parameters for each spectrum to achieve a good continuum fit. The parameters that can be adjusted in our approach are the lower and upper σ -clipping factors, the number of σ -clipping iterations, and the LOESS smoothing parameter, α , which corresponds to the fraction of total number of data points that are used in each local fit.

In Fig. 2, we illustrate the continuum fitting process for a hot (HD 27295, $T_{\text{eff}} \sim 11\,000$ K) and a cold star (HD 205512, $T_{\text{eff}} \sim 4\,700$ K) as examples; similar figures for the other SMARTY stars

² For the optical wavelengths, Coelho (2014) has shown that the flux differences between the synthetic and the MILES similar parameters stars are within 2% for stars with $T_{\text{eff}} \geq 6\,250$ K, and 5% for stars with $T_{\text{eff}} \geq 4\,750$ K, but can reach 50% for colder stars.

³ Locally Estimated Scatterplot Smoothing: a non-parametric method for local polynomial regression. We used the task loess from the stats R package (R Core Team 2021).

are shown in Appendix A. The same approach was adopted to fit the continuum of the reference stars to obtain F_C . Before fitting the continuum, all spectra were degraded to the same resolution of $R = 1\,300$. The initial resolution of SMARTY spectra, shown in Fig. 3, was obtained from the arc lamp spectra.

The continuum-corrected SMARTY spectra were multiplied by a factor so that the total flux within the J , H , and K bands (F_J , F_H , and F_K) of our final spectra is consistent with that of the 2MASS photometry; i.e., the factor was chosen so that it leads to $(F_J + F_H + F_K)_{\text{SMARTY}} = (F_J + F_H + F_K)_{\text{2MASS}}$.

The line-of-sight velocities used to correct the SMARTY spectra were determined through cross-correlation with the theoretical spectra using the task `xcsao` from the `iraf rvsao` package (for details, see Tonry & Davis 1979; Kurtz et al. 1992; Mink & Kurtz 1998). To avoid the regions with telluric contamination, the cross-correlation was performed separately within the J , H , and K wavelength ranges, and we adopted the result with the lowest uncertainty.

The flux-corrected SMARTY spectra are available at www.if.ufrgs.br/~riffel/smarty/. We recommend using SMARTY with the continuum from the common stars when available, from interpolated stars when $T_{\text{eff}} \lesssim 7500\,\text{K}$, and from synthetic stars when $T_{\text{eff}} \gtrsim 7500\,\text{K}$.

3.1 Comparison with literature data

To assess the uncertainties of our approach, in Fig. 4, we show the SMARTY spectra calibrated using F_C from the common, interpolated and synthetic stars (as listed above). In this figure, we show the five stars that also have spectra available in other NIR libraries, and to evaluate possible differences in a more quantitative way, we computed the pixel deviation following the equation:

$$\Delta = \frac{(F_S - F)}{F}, \quad (1)$$

where F_S is the flux of the SMARTY star (for each of the independent calibration procedures), and F is the flux of the common star (taken from the different libraries). We show the mean value of the pixel deviation ($\bar{\Delta}$) and its standard deviation (σ_{Δ}) for the three independent flux calibration procedures in the different windows. As can be seen, there is a very good agreement for all 5 stars, with differences up to $\bar{\Delta} = 0.03$ (for H -band of HD 087822), but for almost all the cases, $\bar{\Delta} \sim 0.01$.

3.2 Index comparisons

The equivalent widths (EW) of absorption lines are one of the most adequate ways to compare the underlying spectrum of stars. To better compare the SMARTY spectra with the predictions of their synthetic and interpolated versions, we have measured the EW of the ions of H I, Mg I, Fe I, Mn I, Al I, Si I, Na I, Ca I and molecular absorptions of CN and CO. For this, we have used a Python modified version of the code `PACCE` (Riffel & Borges Vale 2011) with the definitions for the indices presented in (Riffel et al. 2019), except for the Pa β and Br γ indices, where the definitions of Eftekhari et al. (2021) and Kleinmann & Hall (1986) have respectively been used. Before measuring the EW, all the spectra have been homogenised to a uniform spectral resolution of $R = 1\,300$ (see Fig. 3).

In Fig. 5, we compare the indices measured in the SMARTY with the predicted values of the interpolated and synthetic spectra. We show the measured value, for each index, in the SMARTY stars in the x-axis and the difference between the SMARTY stars with those measured (Δ) in the synthetic spectra (crosses) and the interpolated ones (circles)

in the y-axis. The SMARTY measurements are colour-coded according to the star's temperature. The one-to-one relation is represented by the full line, while the standard deviation of the difference between the measurements of the SMARTY and synthetic stars is represented as a dashed line.

In general, there is a good agreement between the SMARTY and other (synthetic and interpolated) values. However, a large spread is observed among different indices. Although for some indices, the standard deviation of the differences (indicated by the dashed lines in Fig. 5) is small, measurements for individual elements in individual stars may show very large differences (see Fig. 6). For instance, the indices Mn I, H I (especially Pa β), and CN are similar for both the SMARTY spectra corrected by interpolated and by synthetic stars, with relative differences within 5%. The worst indices were the CO bands, Si I and Ca I, reaching up to a relative difference of up to 2 times. Also, in some cases, the difference between the synthetic and interpolated measurements is too large (e.g. Si I $\lambda 15\,800\,\text{\AA}$), where the interpolated values are smaller than the synthetic ones, which can reach up to 2 \AA larger than the interpolated ones for the cooler stars.

Taking into account all the indices at the same time, we found that $(\text{EW}_S - \text{EW}_{\text{synth}})/\text{EW}_S = -0.2 \pm 0.84$ and $(\text{EW}_S - \text{EW}_{\text{interp}})/\text{EW}_S = -0.13 \pm 0.81$, indicating that, within the errors, both interpolated and synthetic spectra are in good agreement, with the interpolated EW predictions being somehow in better agreement than those obtained from the synthetic ones.

Finally, the source of these discrepancies is unclear, and addressing them is out of the scope of this study. However, we speculate that regarding the synthetic spectra, the spread may come from differences in the chemical abundance pattern (the synthetic spectra adopt solar-scaled abundances) or inaccuracies in the model opacities (see Coelho 2014; Coelho et al. 2020). In the case of the interpolated stars, the spectrum is computed by mixing observed spectra of different stars (see Vazdekis et al. 2003), thus in terms of individual elements, it may produce some deviations (e.g. differences in elemental abundances may produce different indices).

3.3 Comparison with 2MASS photometry

To check the overall accuracy of the final corrected SMARTY spectra⁴, we compared the spectrophotometric magnitudes derived from the SMARTY spectra with the values available at the 2MASS point source catalogue (PSC, Skrutskie et al. 2006).

In Fig. 7, we compare SMARTY and 2MASS magnitudes in J , H and K bands. We can see that there is a very good agreement between SMARTY and 2MASS magnitudes, with maximum differences that do not exceed $\sim 0.2\,\text{mag}$. The mean differences in magnitude for the stars corrected by interpolated and synthetic spectra are, respectively, -0.01 and $0.0\,\text{mag}$ for the J band; -0.02 and $-0.03\,\text{mag}$ for the H band; and 0.06 and $0.07\,\text{mag}$ for the K band.

The colour indices obtained directly from the SMARTY spectra are compared with the 2MASS ones in Fig. 8, where a good agreement can be observed with the maximum differences being smaller than $\sim 0.3\,\text{mag}$ for all colour indices. However, the SMARTY spectra lead to slightly lower (bluer) colour indices compared to the values from the 2MASS photometry (with mean differences in the range of -0.10 to $-0.07\,\text{mag}$ in both the $J - K$ and $H - K$ indices). Part of this small systematic difference might be due to Galactic extinction corrections,

⁴ We compared the magnitudes from the flux second order calibration of the SMARTY stars, for both corrections, e.g. using the continuum from the interpolated and the theoretical spectra.

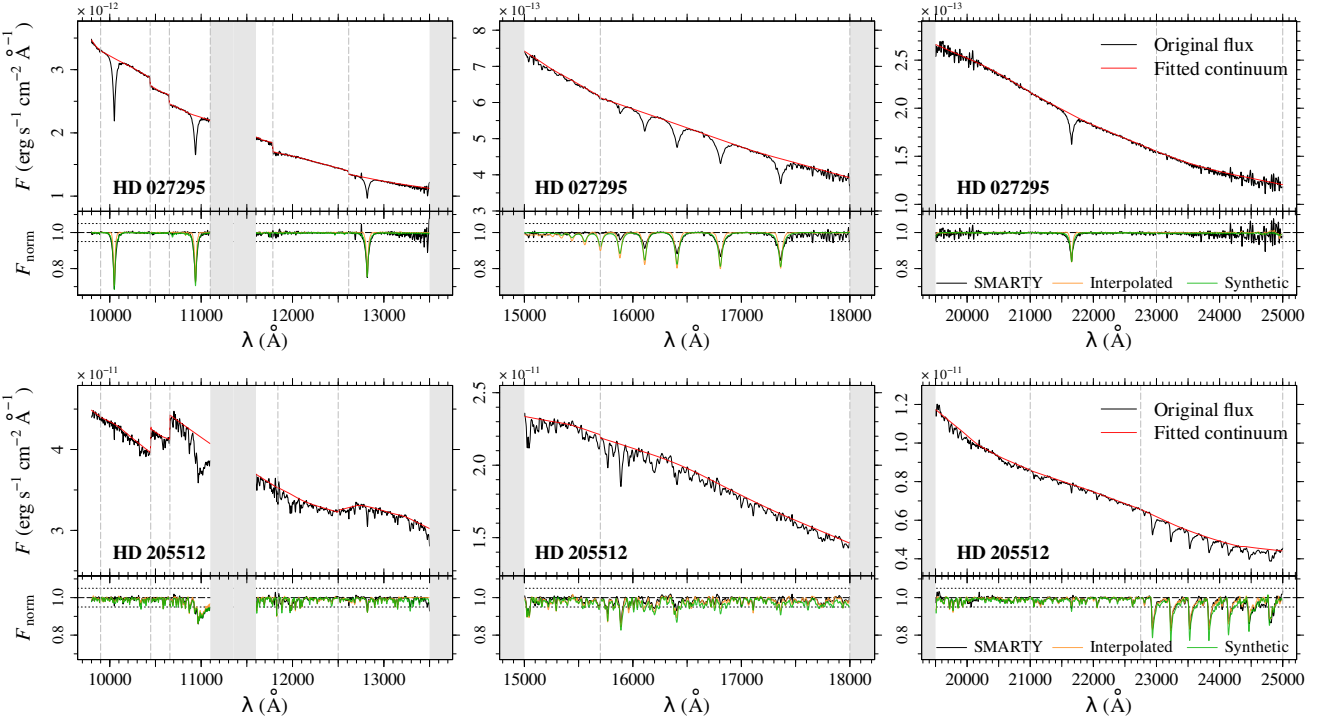


Figure 2. Illustration of the continuum-fit process for a hot (HD 27295, $T_{\text{eff}} \sim 11\,000$ K) and a cold star (HD 205512, $T_{\text{eff}} \sim 4\,700$ K). The upper plot in each panel shows the original flux (black line) and the fitted continuum (red line), and the lower plot shows the resulting normalised flux. The normalised spectra of the synthetic and interpolated stars in the lower plots are also shown as the orange and green lines, respectively. To properly fit the continuum of different spectral regions and to correct the ‘steps’ in the flux that could not be removed during the data reduction, the fit was done independently within wavelength ranges indicated by the vertical grey dashed lines (see text for details). The figures showing the fitted continuum for all the stars are in the Appendix A (Fig.A1).

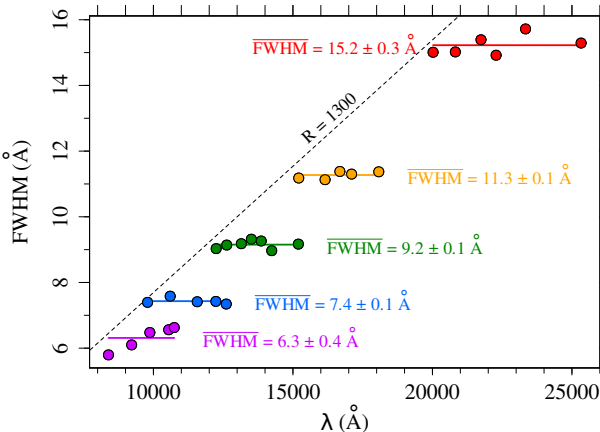


Figure 3. GNIRS spectral resolution as a function of wavelength, which is assumed to be the initial resolution of SMARTY spectra. The SMARTY spectra are convolved to constant $R = 1\,300$, indicated by the dashed line.

which are not applied to the 2MASS magnitudes, but, since we use the continuum from the reference stars, the SMARTY spectra are “implicitly” extinction corrected.

To estimate the impact of the extinction corrections on the colour comparisons, we computed the colour differences for stars with $E(B-V) \simeq 0$ only; we find that the differences between SMARTY and 2MASS colours are smaller for these stars, with $\Delta(J-K) = 0.00 \pm 0.09$ (-0.03 ± 0.07) and $\Delta(H-K) = -0.06 \pm 0.06$ (-0.09 ± 0.05) for SMARTY stars with continuum corrected using the interpolated (synthetic) stars. On the other hand, $\Delta(J-H)$ in-

creases to 0.06 ± 0.07 (0.05 ± 0.07). We also obtained extinction estimates in the J , H , and K bands by Schlegel et al. (1998)⁵ and corrected the 2MASS magnitudes and colours. After applying the corrections, the differences between SMARTY and 2MASS colours decrease to $\Delta(J-K) = 0.04 \pm 0.14$ (0.04 ± 0.13) and $\Delta(H-K) = -0.04 \pm 0.08$ (-0.06 ± 0.07). However, $\Delta(J-H)$ increases to 0.09 ± 0.12 (0.10 ± 0.12).

4 FINAL REMARKS

We presented a stellar spectral library with 31 stars covering the wavelength range from 0.9 to $2.4\,\mu\text{m}$ observed with GNIRS at Gemini North Telescope. The SMARTY is publicly available at www.if.ufrgs.br/~riffel/smarty/. To ensure the spectra quality, we corrected the flux using the continuum of reference stellar spectra from three different sources: *i*) stars in common with other NIR empirical libraries; *ii*) spectra obtained through interpolation of the empirical IRTF+EIRTF library; and *iii*) theoretical spectra based on Coelho et al. (2020), extended to cover our wavelength range.

The average flux difference between SMARTY and the reference spectra is $\lesssim 2\%$, as can be seen in Fig. 4, where we compare the SMARTY spectra corrected with the continuum from the three sources mentioned above with the spectra of stars in common with other libraries.

⁵ Extinction estimated were obtained through the NASA/IPAC Infrared Science Archive (IRSA) web tool available at <https://irsa.ipac.caltech.edu/applications/DUST/>. These estimates correspond to the total reddening along the line of sight, and the distances to the stars are not considered.

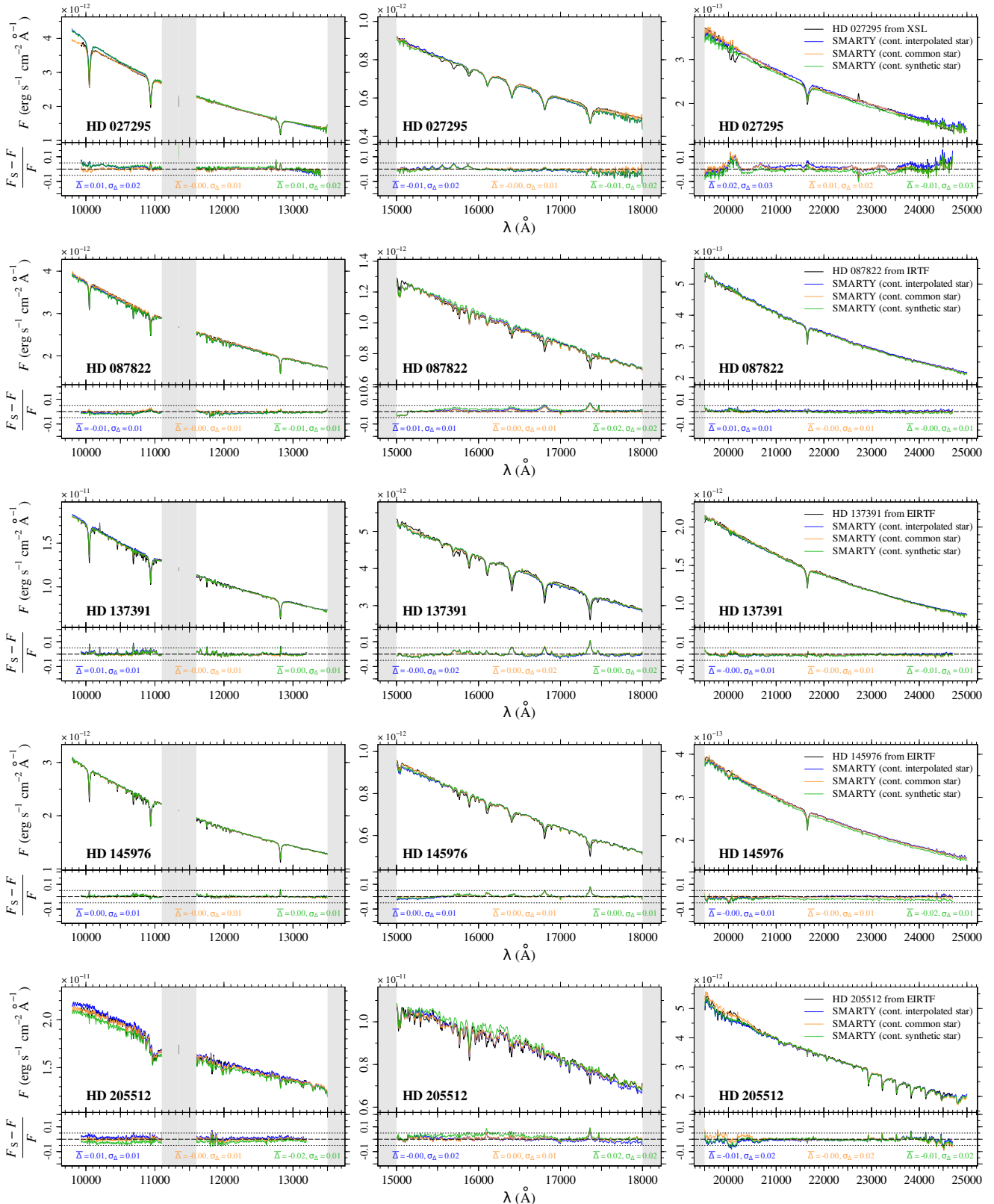


Figure 4. Comparison between SMARTY and the reference spectra from XSL, IRTF or EIRTF for the five stars in common with these libraries. The upper plot in each panel is the flux, and the lower plot shows the relative difference between the SMARTY and reference spectra. The dashed and dotted lines indicate 0 ± 0.05 , respectively. The shaded areas are omitted due to telluric contamination.

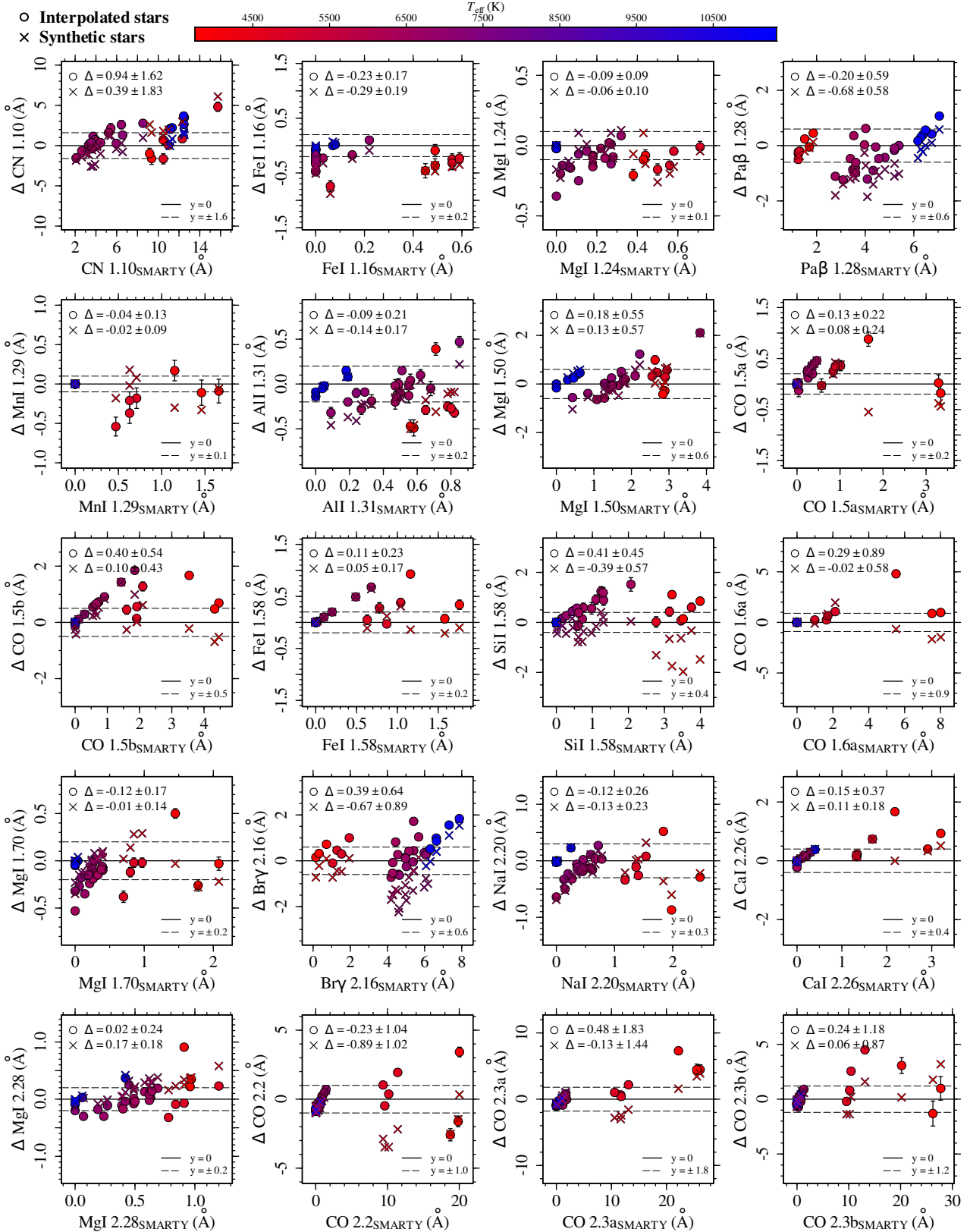


Figure 5. Differences between spectral indices measured in SMARTY and the interpolated (circles) and the synthetic (crosses) stellar spectra vs. values obtained for SMARTY. The symbols are colour-coded by effective temperature, and the error bars are shown for the measurements made in SMARTY spectra with the continuum from interpolated stars. In each panel, for each set of measurements, we show the mean and standard deviation of the differences between SMARTY and interpolated and synthetic measurements ($\Delta \pm \sigma_\Delta$). The solid and the dashed lines represent $y = 0$ and $y = \pm \sigma_\Delta$, where σ_Δ is the standard deviation of the differences between the SMARTY spectral indices and those from interpolated stellar spectra.

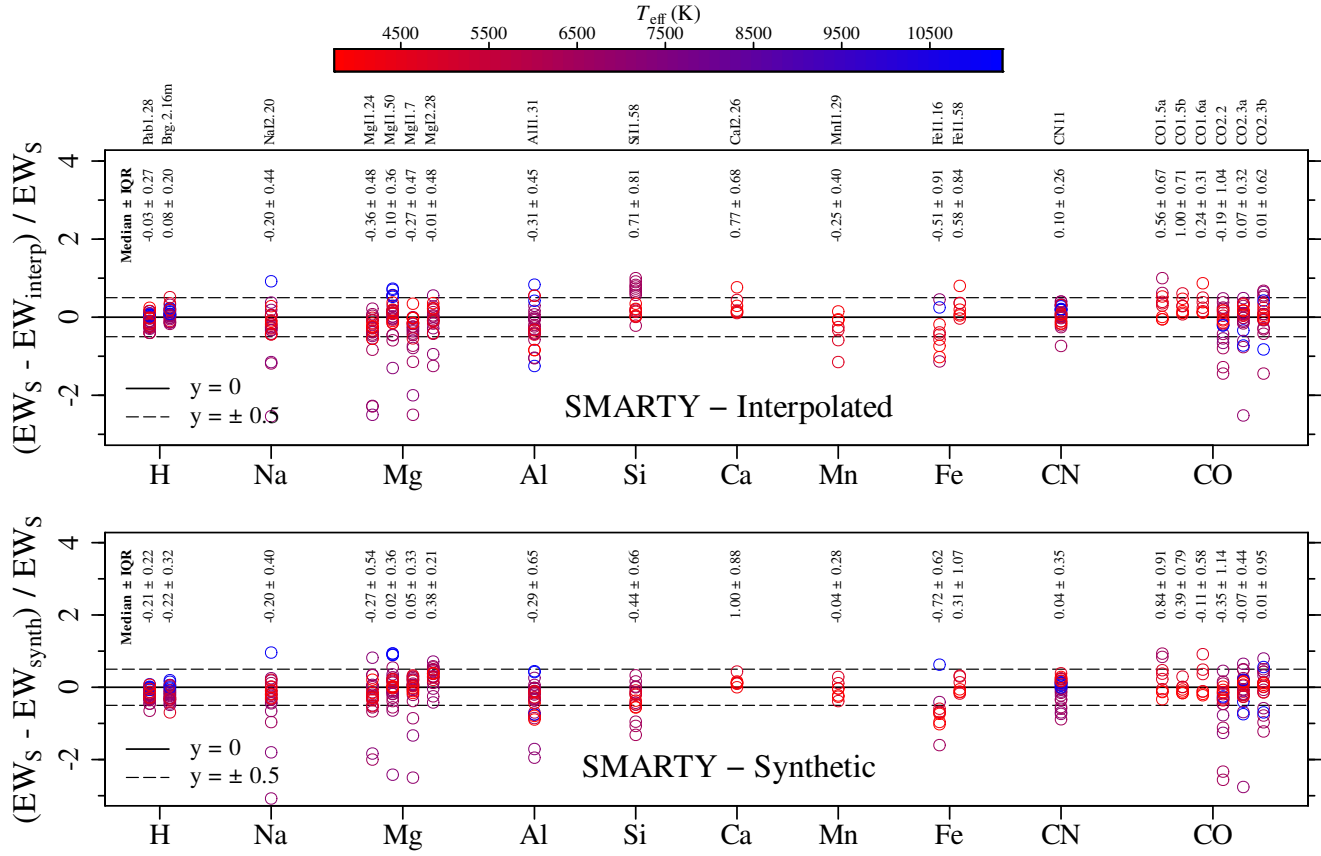


Figure 6. Relative differences between SMARTY spectral indices and those measured in the interpolated (upper panel) and the synthetic (lower panel) stellar spectra, grouped by chemical element or molecule. In both panels, the symbols are colour-coded by effective temperature. The figure shows only stars for which $\text{EW}/\sigma_{\text{EW}} \geq 2$, where EW and σ_{EW} are the SMARTY index value and its uncertainty, respectively. The median values and interquartile ranges (IQR) of the relative differences are shown for each index.

We also investigated our data reliability by comparing the equivalent widths measured in the SMARTY spectra with those obtained from synthetic spectra computed with the atmospheric parameters of the SMARTY stars and interpolated from the IRTF+EIRTF stars. We find good agreement between the EW values; however, large differences can be observed for a few individual stars.

We have also compared the magnitudes and colour indices from SMARTY spectra with those from 2MASS photometry. The comparison reveals a very good agreement between SMARTY and 2MASS magnitudes, with mean differences from -0.01 to 0.07 mag and standard deviation from 0.04 to 0.07 mag in the J , H , and K bands. A good agreement is also observed for the colour indices, with mean differences from -0.10 to 0.03 mag for the $(J - H)$, $(J - K)$, and $(H - K)$ indices. A small difference was noted between the SMARTY spectra corrected using the continuum from the interpolated and the theoretical stars.

ACKNOWLEDGEMENTS

We thank the anonymous referee for the valuable feedback, which greatly improved this manuscript. We thank Alan Alves Brito and Alejandra Romero for their helpful comments and discussions. MBC acknowledges support from Fundação de Amparo à Pesquisa do Rio Grande do Sul (FAPERGS) and Coordenação de Aperfeiçoamento de

Pessoal de Nível Superior (CAPES). RR acknowledges support from the Fundación Jesús Serra and the Instituto de Astrofísica de Canarias under the Visiting Researcher Programme 2023–2025 agreed between both institutions. RR also acknowledges support from the ACI-ISI, Consejería de Economía, Conocimiento y Empleo del Gobierno de Canarias and the European Regional Development Fund (ERDF) under grant with reference ProID2021010079, and the support through the RAVET project by the grant PID2019-107427GB-C32 from the Spanish Ministry of Science, Innovation and Universities MCIU. This work has also been supported through the IAC project TRACES, which is partially supported through the state budget and the regional budget of the Consejería de Economía, Industria, Comercio y Conocimiento of the Canary Islands Autonomous Community. RR also thanks to Conselho Nacional de Desenvolvimento Científico e Tecnológico (CNPq, Proj. 311223/2020-6, 304927/2017-1 and 400352/2016-8), FAPERGS (Proj. 16/2551-0000251-7 and 19/1750-2), and CAPES (Proj. 0001). MT thanks the support from CNPq (process 312541/2021-0). LGDH acknowledges support by National Key R&D Program of China No.2022YFF0503402. PC acknowledges support from CNPq under grant 310555/2021-3 and from Fundação de Amparo à Pesquisa do Estado de São Paulo (FAPESP) process number 2021/08813-7. DRD acknowledges support from CNPq under grant 313040/2022-2. AV acknowledges support from

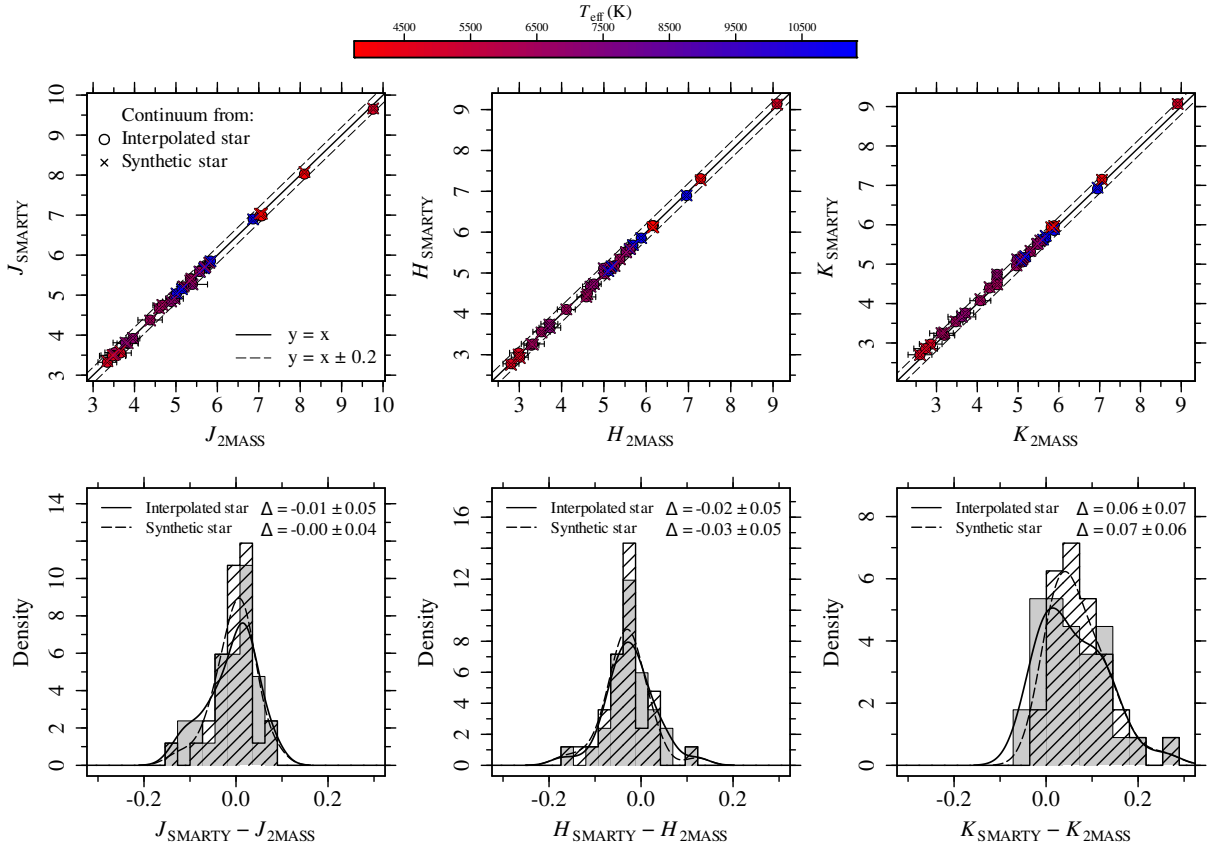


Figure 7. Comparison between the 2MASS magnitudes with those from the SMARTY spectra corrected using as the continuum from the interpolated (circles) and theoretical stars (crosses), colour-coded by effective temperature. **Upper panels:** J , H , and K magnitudes from the SMARTY spectra vs. 2MASS magnitudes. The black solid and dashed lines indicate $y = x$ and $y = x \pm 0.2$, respectively. **Bottom panels:** distributions of the differences between the 2MASS and SMARTY magnitudes obtained with SMARTY spectra corrected using the interpolated (filled grey histograms) and theoretical stars (black hashed histograms). The distribution mean values and standard deviations are indicated in each panel. The solid and the dashed lines are obtained by smoothing the positions of the data points using a Gaussian kernel with a standard deviation equal to half of the standard deviation of the data points.

grant PID2021-123313NA-I00 and PID2022-140869NB-I00 from the Spanish Ministry of Science and Innovation.

This publication makes use of data products from the Two Micron All Sky Survey, which is a joint project of the University of Massachusetts and the Infrared Processing and Analysis Center/California Institute of Technology, funded by the National Aeronautics and Space Administration and the National Science Foundation.

DATA AVAILABILITY

The SMARTY presented in this article is available at <https://www.if.ufrgs.br/~riffel/smarty/>. We provide the following information in a single csv file for each star:

- (i) `lambda`: wavelength (\AA);
- (ii) `flux`: rest-frame flux of the SMARTY spectrum corrected using the continuum of the interpolated star ($\text{erg cm}^{-2} \text{s}^{-1} \text{\AA}^{-1}$);
- (iii) `err`: error on the flux corrected using the interpolated star ($\text{erg cm}^{-2} \text{s}^{-1} \text{\AA}^{-1}$);
- (iv) `flux_norm`: normalized SMARTY spectrum;
- (v) `err_norm`: error on the SMARTY normalized spectrum;
- (vi) `flux_cont_interp_star`: the continuum of the interpolated star ($\text{erg cm}^{-2} \text{s}^{-1} \text{\AA}^{-1}$);

(vii) `flux_corr_synt`: rest-frame flux of the SMARTY spectrum corrected using the continuum of the synthetic star ($\text{erg cm}^{-2} \text{s}^{-1} \text{\AA}^{-1}$);

(viii) `err_corr_synt`: error on the SMARTY flux corrected using the synthetic star ($\text{erg cm}^{-2} \text{s}^{-1} \text{\AA}^{-1}$);

(ix) `flux_cont_synt`: the continuum of the synthetic star ($\text{erg cm}^{-2} \text{s}^{-1} \text{\AA}^{-1}$);

(x) `flux_orig`: flux of the original SMARTY spectrum ($\text{erg cm}^{-2} \text{s}^{-1} \text{\AA}^{-1}$);

(xi) `err_orig`: error on the flux of the original SMARTY spectrum;

(xii) `flux_cont_orig`: continuum of the original SMARTY spectrum;

(xiii) `flux_corr_ref`: rest-frame flux of the SMARTY spectrum corrected using the continuum of the star in common with other libraries *when available* ($\text{erg cm}^{-2} \text{s}^{-1} \text{\AA}^{-1}$);

(xiv) `err_corr_ref`: error on the SMARTY spectrum corrected using the star in common with other libraries *when available*;

(xv) `flux_cont_ref`: continuum of the star in common with other libraries *when available* ($\text{erg cm}^{-2} \text{s}^{-1} \text{\AA}^{-1}$).

REFERENCES

Arentsen A., et al., 2019, *A&A*, **627**, A138

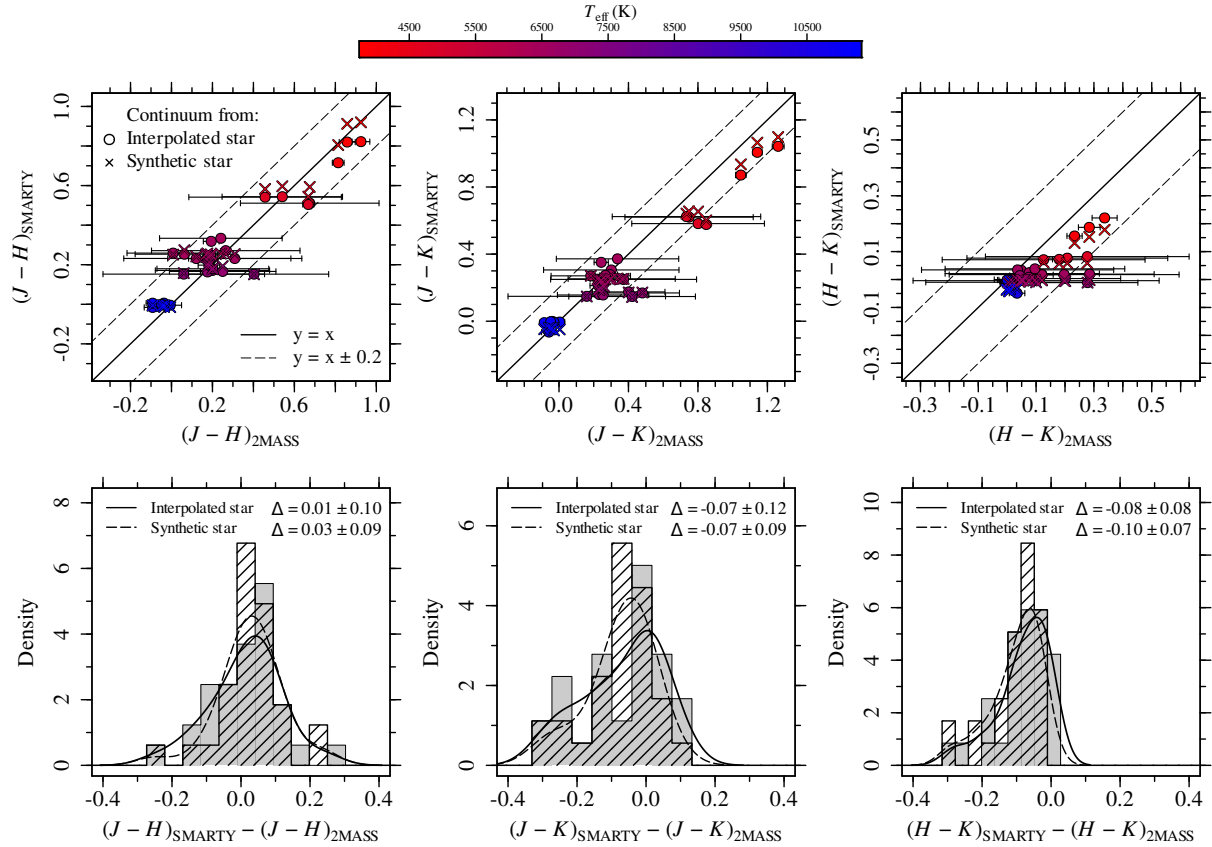


Figure 8. Comparison between the 2MASS colour indices with those from the SMARTY spectra corrected using as the continuum from the interpolated (circles) and theoretical stars (crosses), colour-coded by effective temperature. **Upper panels:** $(J - H)$, $(J - K)$, and $(H - K)$ from the SMARTY spectra vs. 2MASS colour indices. The *black solid* and *dashed lines* indicate $y = x$ and $y = x \pm 0.2$, respectively. **Bottom panels:** distributions of the differences between the 2MASS and SMARTY magnitudes obtained with SMARTY spectra corrected using the interpolated (filled grey histograms) and theoretical stars (black hashed histograms). The distribution mean values and standard deviations are indicated in each panel. The *solid* and the *dashed lines* are obtained by smoothing the positions of the data points using a Gaussian kernel with a standard deviation equal to half of the standard deviation of the data points.

- Boyett K., et al., 2024, arXiv e-prints, p. arXiv:2401.16934
 Cappellari M., 2023, MNRAS, 526, 3273
 Cenarro A. J., et al., 2007, MNRAS, 374, 664
 Chen Y.-P., Trager S. C., Peletier R. F., Lançon A., Vazdekis A., Prugniel P.,
 Silva D. R., Gonneau A., 2014, A&A, 565, A117
 Coelho P., 2009, in Giobbi G., Tornambe A., Raimondo G., Limongi M.,
 Antonelli L. A., Menci N., Brocato E., eds, American Institute of Physics
 Conference Series Vol. 1111, Probing Stellar Populations Out to the
 Distant Universe: Cefalu 2008, Proceedings of the International Conference.
 pp 67–74 (arXiv:0906.1020), doi:10.1063/1.3141624
 Coelho P. R. T., 2014, Monthly Notices of the Royal Astronomical Society,
 440, 1027
 Coelho P. R. T., Bruzual G., Charlot S., 2020, MNRAS, 491, 2025
 Conroy C., 2013, ARA&A, 51, 393
 Conroy C., Gunn J. E., White M., 2009, ApJ, 699, 486
 Conselice C. J., 2014, ARA&A, 52, 291
 Cushing M. C., Rayner J. T., Vacca W. D., 2005, ApJ, 623, 1115
 Dahmer-Hahn L. G., Riffel R., Rodríguez-Ardila A., Martins L. P., Kehrig C.,
 Heckman T. M., Pastoriza M. G., Dametto N. Z., 2018, Monthly Notices
 of the Royal Astronomical Society, 476, 4459
 Dahmer-Hahn L. G., et al., 2019, MNRAS, 482, 5211
 Dametto N. Z., Riffel R., Pastoriza M. G., Rodríguez-Ardila A., Hernandez-
 Jimenez J. A., Carvalho E. A., 2014, Monthly Notices of the Royal
 Astronomical Society, 443, 1754
 Eftekhari E., Vazdekis A., La Barbera F., 2021, MNRAS, 504, 2190
 Eftekhari E., La Barbera F., Vazdekis A., Allende Prieto C., Knowles A. T.,
 2022, MNRAS, 517, 4379
 Falcón-Barroso J., Sánchez-Blázquez P., Vazdekis A., Ricciardelli E., Cardiel
 N., Cenarro A. J., Gorgas J., Peletier R. F., 2011, A&A, 532, A95
 Fernandes R. C., Mateus A., Sodré L., Stasińska G., Gomes J. M., 2005,
 Monthly Notices of the Royal Astronomical Society, 358, 363
 García Pérez A. E., et al., 2021, MNRAS, 505, 4496
 Gasparri D., et al., 2021, MNRAS, 507, 4669
 Gasparri D., et al., 2024, MNRAS,
 Gomes J. M., Papaderos P., 2017, A&A, 603, A63
 Gonneau A., et al., 2020, A&A, 634, A133
 Gustafsson B., Edvardsson B., Eriksson K., Jørgensen U. G., Nordlund Å.,
 Plez B., 2008, A&A, 486, 951
 Husser, T.-O. Wende-von Berg, S. Dreizler, S. Homeier, D. Reiners, A. Bar-
 man, T. Hauschildt, P. H. 2013, A&A, 553, A6
 Kleinmann S. G., Hall D. N. B., 1986, ApJS, 62, 501
 Knowles A. T., Sansom A. E., Allende Prieto C., Vazdekis A., 2021, MNRAS,
 504, 2286
 Knowles A. T., Sansom A. E., Vazdekis A., Allende Prieto C., 2023, MNRAS,
 523, 3450
 Kotilainen J. K., Hyvönen T., Reunanen J., Ivanov V. D., 2012, MNRAS,
 425, 1057
 Kurtz M. J., Mink D. J., Wyatt W. F., Fabricant D. G., Torres G., Kriss
 G. A., Tonry J. L., 1992, in Worrall D. M., Biemesderfer C., Barnes
 J., eds, Astronomical Society of the Pacific Conference Series Vol. 25,
 Astronomical Data Analysis Software and Systems I. p. 432
 Lançon A., et al., 2021, A&A, 649, A97

- Luhman K. L., et al., 2024, *AJ*, **167**, 5
- Maraston C., 2005, *MNRAS*, **362**, 799
- Maraston C., Strömbäck G., 2011, *MNRAS*, **418**, 2785
- Maraston C., Daddi E., Renzini A., Cimatti A., Dickinson M., Papovich C., Pasquali A., Pirzkal N., 2006, *ApJ*, **652**, 85
- Marino A. F., et al., 2024, arXiv e-prints, p. arXiv:2401.06681
- Martins L. P., Rodríguez-Ardila A., Diniz S., Gruenwald R., de Souza R., 2013a, *MNRAS*, **431**, 1823
- Martins L. P., Rodríguez-Ardila A., Diniz S., Riffel R., de Souza R., 2013b, *MNRAS*, **435**, 2861
- Martins L. P., Lima-Dias C., Coelho P. R. T., Laganá T. F., 2019, *MNRAS*, **484**, 2388
- Mason R. E., et al., 2015, *ApJS*, **217**, 13
- McWilliam A., 1997, *ARA&A*, **35**, 503
- Meneses-Goytia S., Peletier R. F., Trager S. C., Falcón-Barroso J., Koleva M., Vazdekis A., 2015, *A&A*, **582**, A96
- Mink D. J., Kurtz M. J., 1998, in Albrecht R., Hook R. N., Bushouse H. A., eds, Astronomical Society of the Pacific Conference Series Vol. 145, Astronomical Data Analysis Software and Systems VII. p. 93
- Moura T. C., Trevisan M., Barbuy B., Rossi S., 2019, *ApJ*, **885**, 28
- Origlia L., Ferraro F. R., Fusi Pecci F., Oliva E., 1997, *A&A*, **321**, 859
- Prugniel P., Vauglin I., Koleva M., 2011, *A&A*, **531**, A165
- R Core Team 2021, R: A Language and Environment for Statistical Computing. R Foundation for Statistical Computing, Vienna, Austria, <https://www.R-project.org>
- Rayner J. T., Cushing M. C., Vacca W. D., 2009, *ApJS*, **185**, 289
- Rennó C., Barbuy B., Moura T. C., Trevisan M., 2020, *MNRAS*, **498**, 5834
- Rieke G. H., Lebofsky M. J., Thompson R. I., Low F. J., Tokunaga A. T., 1980, *ApJ*, **238**, 24
- Riffel R., Borges Vale T., 2011, *Ap&SS*, **334**, 351
- Riffel R., Rodríguez-Ardila A., Pastoriza M. G., 2006, *A&A*, **457**, 61
- Riffel R., Pastoriza M. G., Rodríguez-Ardila A., Maraston C., 2007, *ApJ*, **659**, L103
- Riffel R., Pastoriza M. G., Rodríguez-Ardila A., Maraston C., 2008, *MNRAS*, **388**, 803
- Riffel R., Pastoriza M. G., Rodríguez-Ardila A., Bonatto C., 2009, *MNRAS*, **400**, 273
- Riffel R., Ruschel-Dutra D., Pastoriza M. G., Rodríguez-Ardila A., Santos J. F. C. J., Bonatto C. J., Ducati J. R., 2011a, *MNRAS*, **410**, 2714
- Riffel R., Riffel R. A., Ferrari F., Storchi-Bergmann T., 2011b, *MNRAS*, **416**, 493
- Riffel R., et al., 2015, *MNRAS*, **450**, 3069
- Riffel R., et al., 2019, *Monthly Notices of the Royal Astronomical Society*, **486**, 3228
- Riffel R., et al., 2021, *Monthly Notices of the Royal Astronomical Society*, **501**, 4064
- Riffel R., et al., 2022, *Monthly Notices of the Royal Astronomical Society*, **512**, 3906
- Riffel R., et al., 2023, *Monthly Notices of the Royal Astronomical Society*, **524**, 5640
- Röck B., Vazdekis A., Ricciardelli E., Peletier R. F., Knapen J. H., Falcón-Barroso J., 2016, *A&A*, **589**, A73
- Röck B., Vazdekis A., La Barbera F., Peletier R. F., Knapen J. H., Allende-Prieto C., Aguado D. S., 2017, *MNRAS*, **472**, 361
- Salaris M., Weiss A., Cassarà L. P., Piovan L., Chiosi C., 2014, *A&A*, **565**, A9
- Sánchez S. F., 2020, *Annual Review of Astronomy and Astrophysics*, vol. 58, p.99-155, 58, 99
- Sánchez-Blázquez P., et al., 2006, *MNRAS*, **371**, 703
- Sánchez S. F., et al., 2018, *Revista Mexicana de Astronomía y Astrofísica*, **54**, 217
- Sánchez S. F., Walcher C. J., Lopez-Cobá C., Barrera-Ballesteros J. K., Mejía-Narváez A., Espinosa-Ponce C., Camps-Fariña A., 2021, *Revista Mexicana de Astronomía y Astrofísica*, **57**, 3
- Schlegel D. J., Finkbeiner D. P., Davis M., 1998, *ApJ*, **500**, 525
- Sharma K., Prugniel P., Singh H. P., 2016, *A&A*, **585**, A64
- Silva D. R., Kuntschner H., Lyubenova M., 2008, *ApJ*, **674**, 194
- Skrutskie M. F., et al., 2006, *AJ*, **131**, 1163
- Smette A., et al., 2015, *A&A*, **576**, A77
- Tinsley B. M., 1968, *ApJ*, **151**, 547
- Tody D., 1986, in Crawford D. L., ed., Society of Photo-Optical Instrumentation Engineers (SPIE) Conference Series Vol. 627, Instrumentation in astronomy VI. p. 733, doi:10.1117/12.968154
- Tonry J., Davis M., 1979, *AJ*, **84**, 1511
- Vazdekis A., Cenarro A. J., Gorgas J., Cardiel N., Peletier R. F., 2003, *MNRAS*, **340**, 1317
- Vazdekis A., Ricciardelli E., Cenarro A. J., Rivero-González J. G., Díaz-García L. A., Falcón-Barroso J., 2012, *MNRAS*, **424**, 157
- Vazdekis A., Koleva M., Ricciardelli E., Röck B., Falcón-Barroso J., 2016, *MNRAS*, **463**, 3409
- Verro K., et al., 2022a, *A&A*, **660**, A34
- Verro K., et al., 2022b, *A&A*, **661**, A50
- Villaume A., Conroy C., Johnson B., Rayner J., Mann A. W., van Dokkum P., 2017, *The Astrophysical Journal Supplement Series*, **230**, 23
- Walcher C. J., Coelho P., Gallazzi A., Charlot S., 2009, *MNRAS*, **398**, L44
- Walcher J., Groves B., Budavári T., Dale D., 2011, *Ap&SS*, **331**, 1
- Westera P., Lejeune T., Buser R., Cuisinier F., Bruzual G., 2002, *A&A*, **381**, 524
- Worthey G., Faber S. M., Gonzalez J. J., 1992, *ApJ*, **398**, 69
- Zibetti S., Gallazzi A., Charlot S., Pierini D., Pasquali A., 2013, *MNRAS*, **428**, 1479

APPENDIX A: CONTINUUM FIT

This paper has been typeset from a *TeX/LaTeX* file prepared by the author.

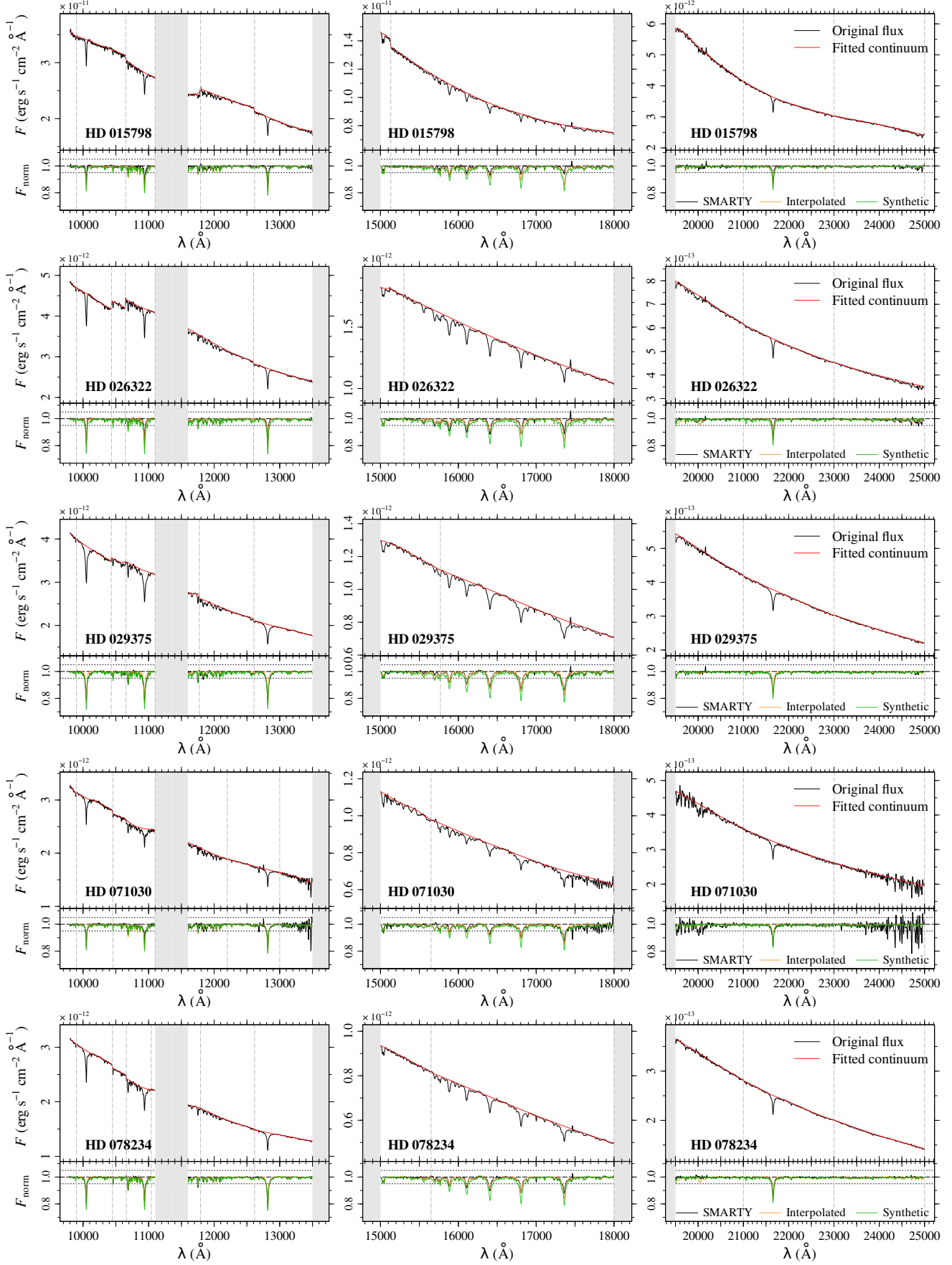


Figure A1. Illustration of the continuum-fit process. The notation is the same as in Fig. 2.

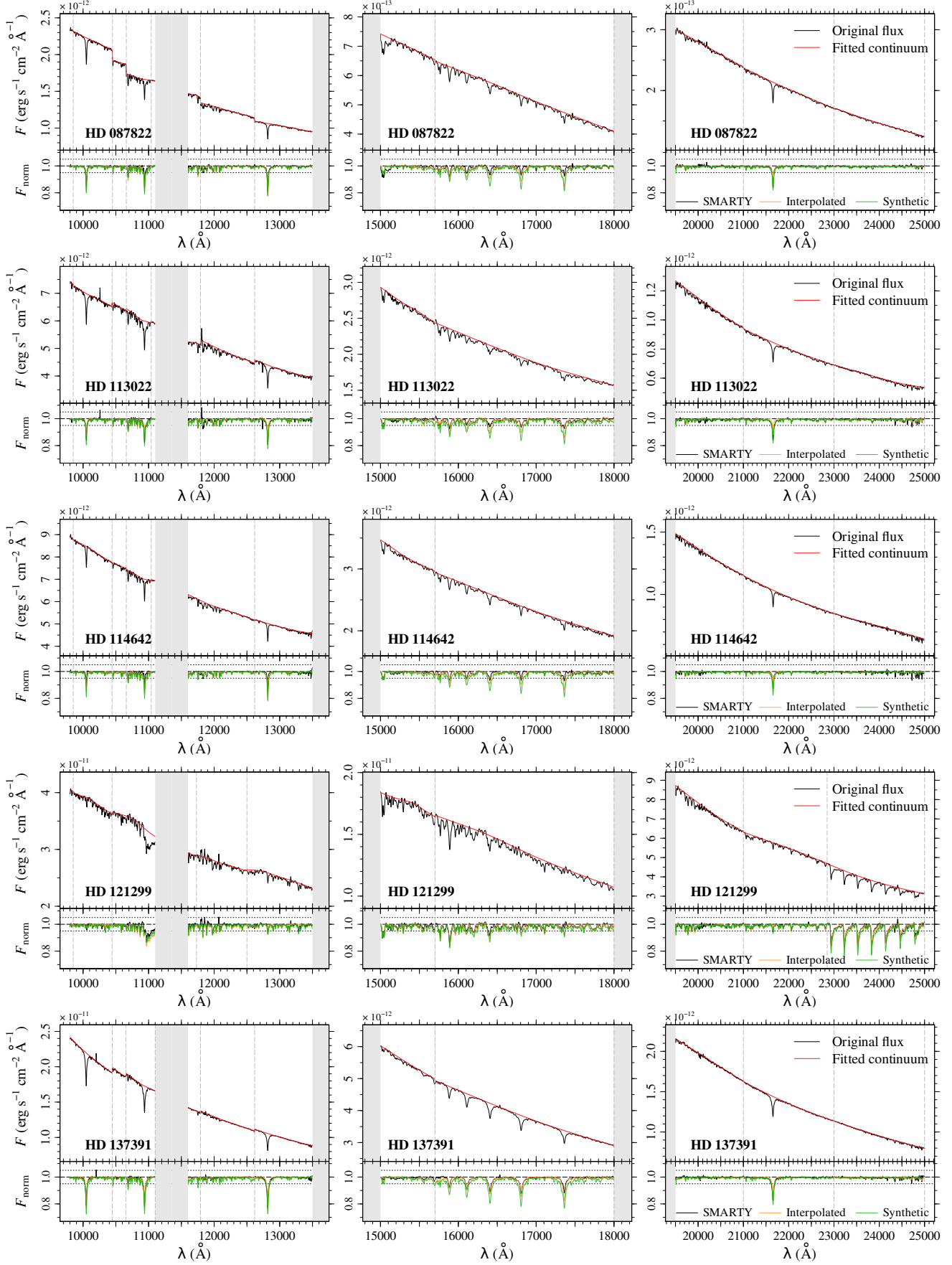


Figure A1 (continued). Illustration of the continuum-fit process. The notation is the same as in Fig. 2.

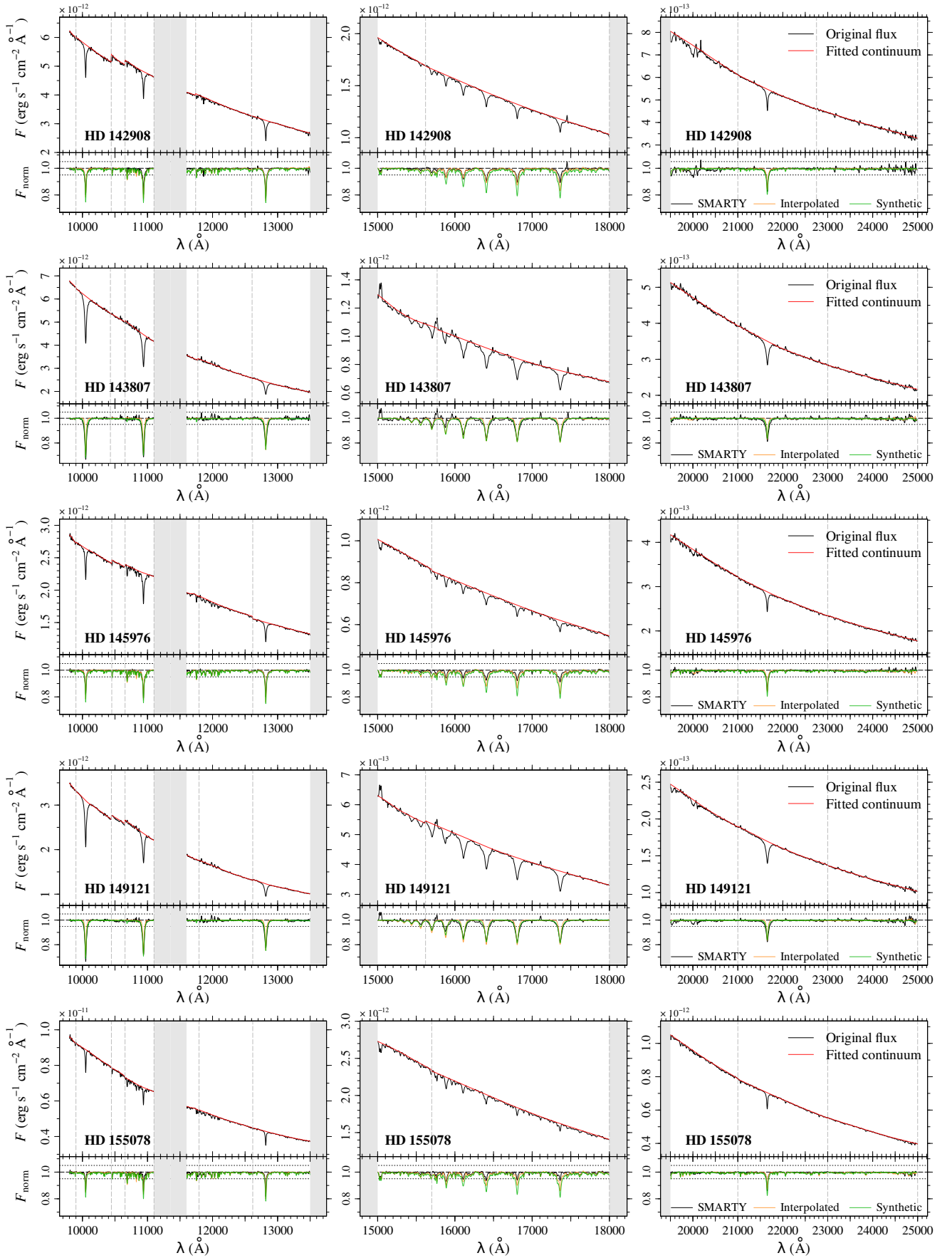


Figure A1 (continued). Illustration of the continuum-fit process. The notation is the same as in Fig. 2.

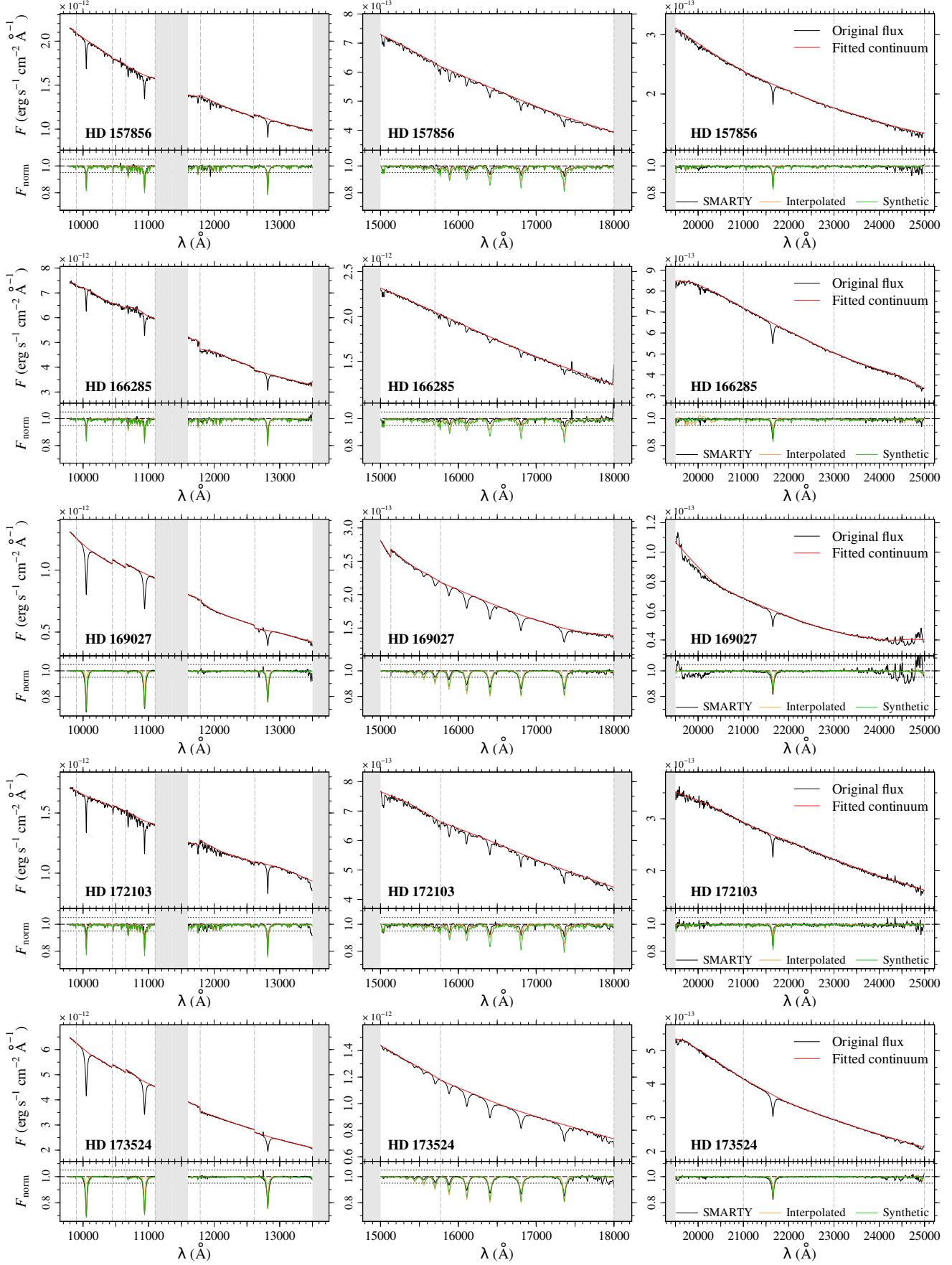


Figure A1 (continued). Illustration of the continuum-fit process. The notation is the same as in Fig. 2.

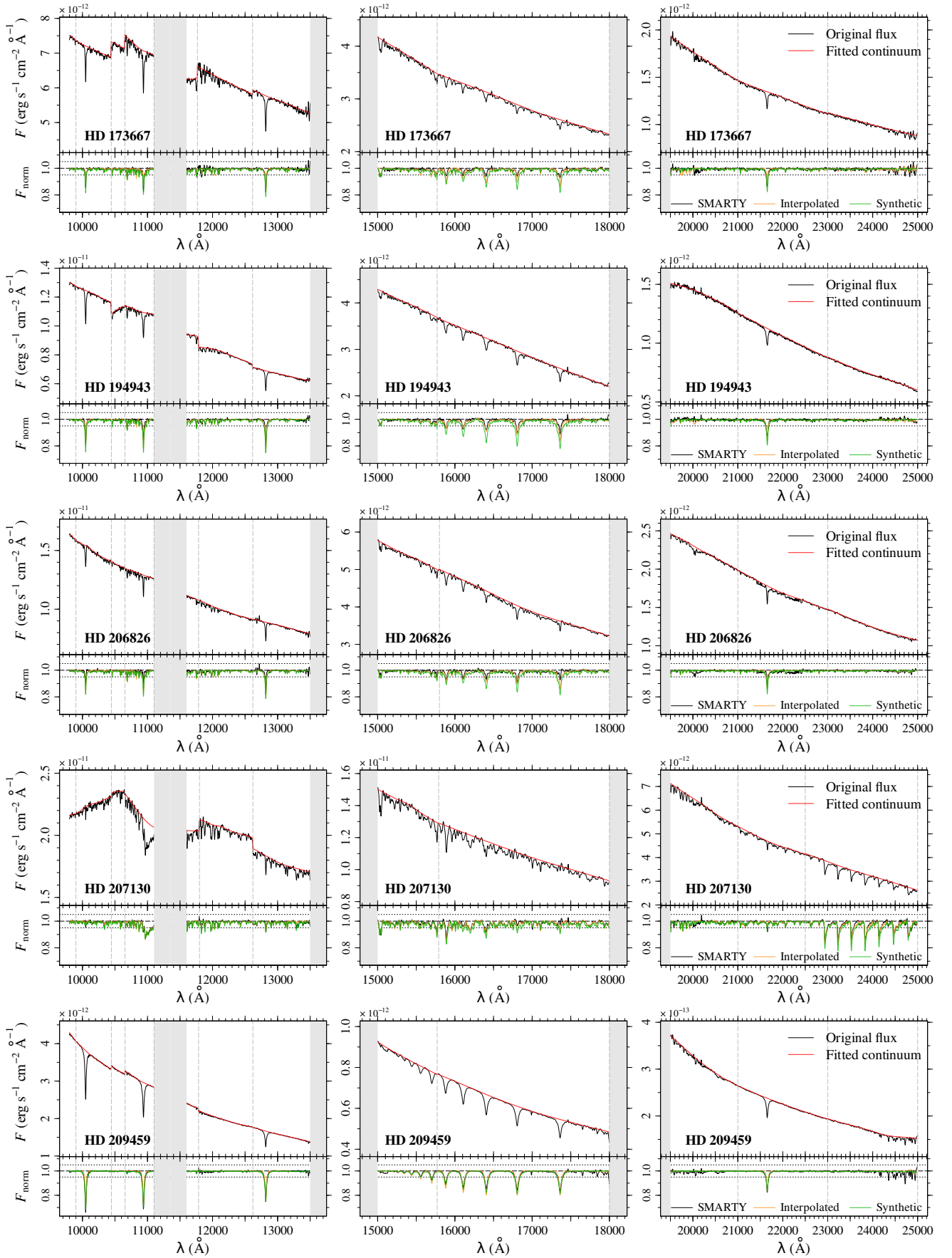


Figure A1 (continued). Illustration of the continuum-fit process. The notation is the same as in Fig. 2.

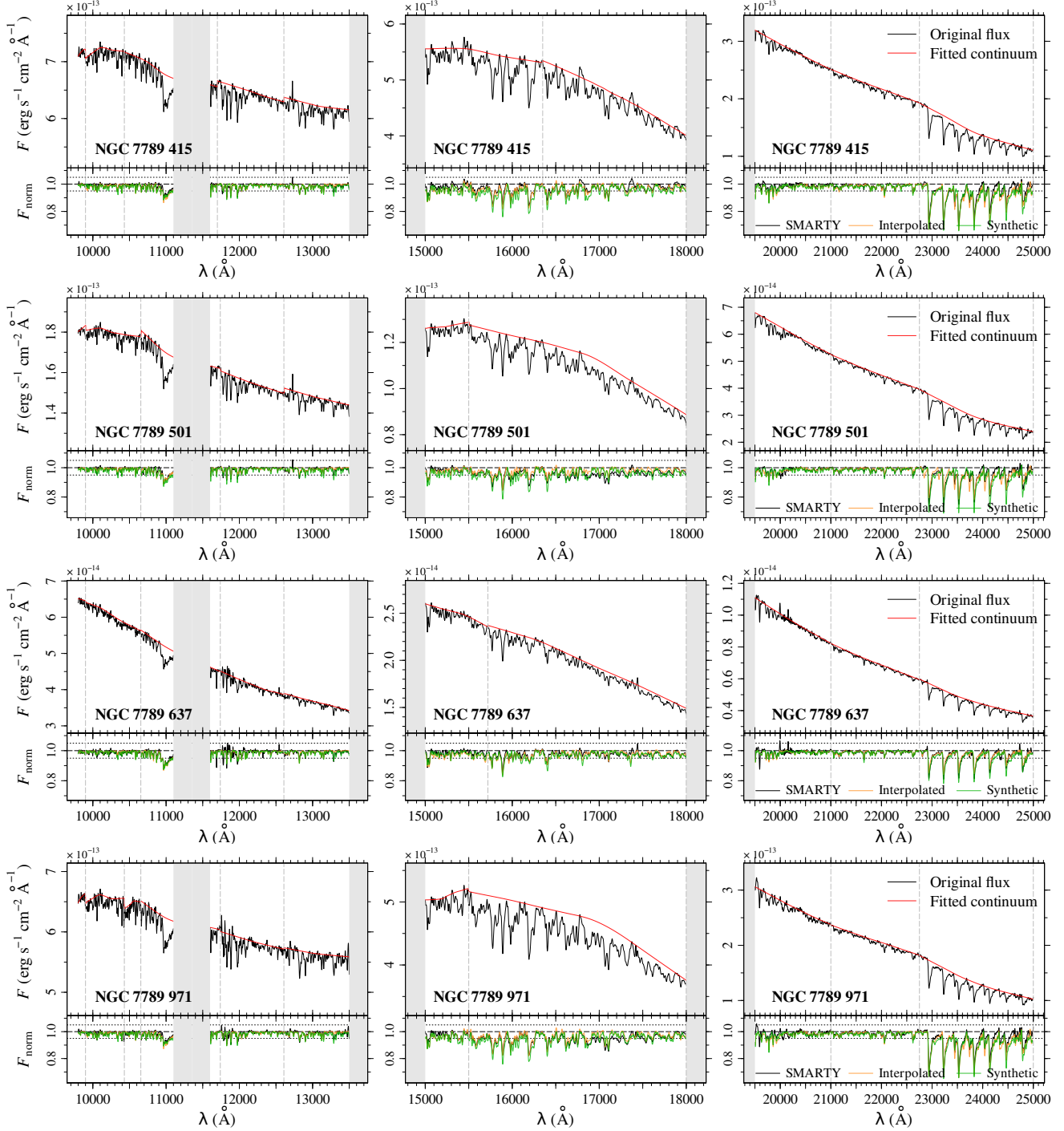


Figure A1 (continued). Illustration of the continuum-fit process. The notation is the same as in Fig. 2.